

# Connecting the one-band and three-band Hubbard models of cuprates via spectroscopy and scattering experiments

K. Sheshadri,<sup>1</sup> D. Malterre,<sup>2</sup> A. Fujimori,<sup>3, 4, 5</sup> and A. Chainani<sup>5</sup>

<sup>1</sup>226, Bagalur, Bangalore North, Karnataka State, India 562149

<sup>2</sup>Institut Jean Lamour, Université de Lorraine, UMR 7198 CNRS, BP70239, 54506 Vandoeuvre lés Nancy, France

<sup>3</sup>Department of Physics, The University of Tokyo,  
7-3-1 Hongo, Bunkyo-ku, Tokyo 113-0033, Japan

<sup>4</sup>Center for Quantum Science and Technology and Department of Physics,  
National Tsing Hua University, Hsinchu 30013, Taiwan

<sup>5</sup>Condensed Matter Physics Group, National Synchrotron Radiation Research Center, Hsinchu 30076, Taiwan

(Dated: November 28, 2022)

The one-band and three-band Hubbard models which describe the electronic structure of cuprates indicate very different values of effective electronic parameters (EPs), such as the Cu on-site Coulomb energy and the Cu-O hybridization strength. In contrast, a comparison of EPs of several cuprates with corresponding values from spectroscopy and scattering experiments indicates similar values in the three-band model and cluster model calculations used to simulate experimental results. To explore this relation in detail, a Cu<sub>2</sub>O cluster model calculation was carried out to obtain an expression for the Heisenberg exchange coupling  $J$  between Cu sites using a downfolding method, taking into account Cu and O on-site correlations ( $U_d$  and  $U_p$ ), the charge-transfer energy  $\Delta$  and the hopping  $t$  between Cu and O sites. A quantitative analysis provides a consistent description of  $J$  from neutron scattering experiments, using the three-band model and spectroscopic EPs. In addition,  $J$  can be expressed in the one-band Hubbard model form with  $\tilde{U}$  and  $\tilde{t}$ , which denote renormalized  $U$  and  $t$  using  $\Delta$  and  $U_p$ , and their values indicate a large  $\tilde{U}/\tilde{t}$ , in agreement with reported values. The large  $\tilde{U}/\tilde{t}$  arising from a combination of  $U_d$ ,  $U_p$  and  $\Delta$  is thus hidden in the effective one-band Hubbard model. The ground-state singlet weights obtained from an exact diagonalization show the importance of the Cu-O Zhang-Rice singlet in the effective one-band Hubbard model. The results provide a consistent method to connect EPs obtained from spectroscopy and the three-band model with values of  $J$  obtained from scattering experiments, band dispersion measurements and the effective one-band Hubbard model.

## I. INTRODUCTION

The mechanism of high-temperature superconductivity exhibited by the copper-oxide families of layered compounds remains one of the most intriguing and challenging topics in condensed matter physics<sup>1</sup>, nearly 36 years after its discovery<sup>2</sup>. The discovery of copper-oxide based superconductivity led to unprecedented theoretical and experimental efforts to understand the phenomenon. While there have been innumerable models put forth to understand the mechanism of high-temperature superconductivity, it still remains an open problem. On the other hand, nearly all the models agree that superconductivity in the copper-oxide based materials is intimately associated with quasi two-dimensionality and strong electron-electron correlations<sup>1</sup>. This is based on the fact that the CuO<sub>2</sub> planes are the main source of the electronic states which undergo the superconducting transition. At a very broad level, the possible mechanisms discussed in the literature span over various models including the effective one-band Hubbard model<sup>3,4</sup>, resonating valence bond theory<sup>5</sup>, the three-band Hubbard model<sup>6,7</sup>, the t-J model<sup>8</sup>, spin-fluctuation driven pairing<sup>9</sup>, marginal Fermi liquid<sup>10</sup>, pair density wave model<sup>11</sup>, electron-phonon coupling-induced pairing which go beyond the BCS model<sup>12</sup>, and so on.

The simplest parent compound La<sub>2</sub>CuO<sub>4</sub> is a good

antiferromagnetic insulator and upon hole-doping, undergoes a transition to a dome shaped superconducting phase with an optimal  $T_c \sim 38$  K<sup>2</sup>. While the long-range order is lost, La<sub>2-x</sub>Sr<sub>x</sub>CuO<sub>4</sub>, as well as several other copper oxide superconductors, continue to exhibit antiferromagnetic correlations in the form of resonant modes and paramagnons in the superconducting phase<sup>13-15</sup>. In fact, along with superconductivity, all the families of copper oxide superconductors also show spin- and charge-ordering phenomena<sup>16-25</sup> which suggest a complex co-existence of electron-phonon coupling, spin fluctuations and electron-electron correlation effects<sup>26,27</sup>.

The basic starting point to understand cuprate properties is often considered to be the two-dimensional Hubbard model involving strong electron-electron correlations with strong Cu-O hybridization leading to the Zhang-Rice singlet (ZRS) ground state<sup>4</sup>. It is well-known and well-accepted that the parent copper-oxide materials are best described as charge-transfer insulators in the Zaanen-Sawatzky-Allen scheme<sup>28</sup>, with the copper on-site Coulomb energy  $U_d \gg \Delta$ , the charge-transfer energy, and the lowest energy excitations involve the strongly hybridized Cu-3d and O-2p ZRS states. Further, hole doping in the parent compound results in oxygen hole carriers retaining the ZRS character of the lowest energy excitations<sup>29-31</sup>. Surprisingly, many theoretical studies have neglected oxygen on-site Coulomb energy  $U_p$ , based on the assumption it is too weak to be of

importance. However, electron spectroscopy studies in conjunction with cluster model calculations or using the Cini-Sawatzky method<sup>32,33</sup> have estimated  $U_d \sim 6 - 8$  eV<sup>34-36</sup> and  $U_p \sim 5 - 6$  eV<sup>37-39</sup>. Thus,  $U_d$  and  $U_p$  are comparable and both need to be considered for describing the electronic states derived from Cu-O planes, particularly in the charge transfer limit, as  $U_p$  gets close to or larger than  $\Delta$ .

A very important issue involves how to quantify electron-electron correlations in any transition metal compound, in general, and the cuprates, in particular<sup>40,41</sup>. Depending on the theoretical model, the values of electron-electron correlation strength can be very different for the same material. A comparison of the effective one band Hubbard model<sup>3,4</sup> consisting of the single antibonding band made up of the Cu  $d_{x^2-y^2}$  and O  $p_x, p_y$  orbitals, and the effective three band Hubbard model<sup>6,7</sup> which describes the cuprate electronic structure in terms of the Cu-O bonding, non-bonding and anti-bonding bands show significantly different values of on-site Coulomb energy  $U_d$  in the Cu  $d$  states. For example, typical values of  $U_d \sim 3-4$  eV is known for the effective one-band model<sup>45,46</sup> while early studies of the three band model estimated  $U_d \sim 7 - 10$  eV and  $U_p \sim 3 - 6$  eV<sup>42-44</sup>.

More recently, an *ab initio* method with dynamical screening<sup>45</sup> applied to the one-band model for La<sub>2</sub>CuO<sub>4</sub> estimated a static  $U_d(w = 0) \sim 3.65$  eV, while for the three-band model, it gave  $U_d(w = 0) \sim 7.0$  eV and  $U_p(w = 0) \sim 4.64$  eV. Another very recent multi-scale *ab initio* method<sup>46</sup> applied to the one band model for

La<sub>2</sub>CuO<sub>4</sub> estimated  $U_d \sim 5.0$  eV, while for the three-band model it estimated  $U_d(w = 0) \sim 9.61$  eV and  $U_p(w = 0) \sim 6.13$  eV. It is noted that the models have also estimated the inter-site Coulomb energies, as well as the nearest and next-nearest-neighbour hopping ( $t$  and  $t'$ ) which also show differences depending on the method<sup>42-46</sup>. The hopping  $t$  shows significant differences in the one-band and three-band cases (see Tables 1 and 2) since  $t$  defines different quantities (Cu-Cu versus Cu-O hopping) in the two models. Very interestingly, Hubbard-type cluster models employing  $d_{x^2-y^2}$ ,  $p_x$  and  $p_y$  levels have been extensively used for calculating spectra in high energy spectroscopies like core-level photoemission (PES) and x-ray absorption (XAS), resonant inelastic x-ray scattering structure factors, etc. and the obtained electronic parameters<sup>37-39,51-66</sup> are quite close to the theoretical estimates from the effective three-band model<sup>42-44,46,67</sup> (see Tables 1 and 2). It is noted that the effective three-band model parameters were also used to calculate the dynamical spin structure factor of Bi2201 measured by RIXS<sup>66</sup>. On the other hand, analysis of neutron scattering measurements of magnon dispersions<sup>48</sup> and angle-resolved photoemission spectroscopy (ARPES) band dispersions<sup>49,50</sup> of parent cuprates have employed the extended one-band Hubbard model or the extended  $t - J$  model to study the nearest neighbor exchange interaction and correlation effects, and they obtained electronic parameter values close to the values obtained from the effective one-band theoretical models.

TABLE I: Electronic parameters ( $\bar{U}_d$ ,  $\bar{t}$ ,  $\bar{\Delta}$ ,  $\bar{U}_p$ ) for cuprates from the three-band Hubbard model (Theory) and from cluster model calculations (Spectroscopy and RIXS). The table also shows two optimized parameter sets ( $\Delta$  and  $U_p$ ) and ( $t$  and  $\Delta$ ) with their cost functions  $f_1$  and  $f_2$ , respectively.  $J$  is the nearest-neighbor Heisenberg exchange deduced from scattering experiments. See text for details.

| Compound<br>(ref. no)                                 | $\bar{U}_d$<br>$\pm 0.5$ eV | $\bar{t}$<br>$\pm 0.2$ eV | $\bar{\Delta}$<br>$\pm 1.0$ eV | $\bar{U}_p$<br>$\pm 0.5$ eV | $\Delta$<br>eV | $U_p$<br>eV | $f_1$ | $J$ (ref.no)<br>$\pm 5$ meV | $t$<br>eV | $\Delta$<br>eV | $f_2$ |
|---|-----------------------------|---------------------------|--------------------------------|-----------------------------|----------------|-------------|-------|-----------------------------|-----------|----------------|-------|
| Theory  |                             |                           |                                |                             |                |             |       |                             |           |                |       |
| La <sub>2</sub> CuO <sub>4</sub> (42)                 | 9.4                         | 1.5                       | 3.5                            | 4.7                         | 5.7            | 4.9         | 5.09  | 140 (48)                    | 1.1       | 3.7            | 0.96  |
| La <sub>2</sub> CuO <sub>4</sub> (43)                 | 10.5                        | 1.3                       | 3.6                            | 4.0                         | 4.5            | 4.1         | 1.01  | 140 (48)                    | 1.2       | 3.7            | 0.4   |
| La <sub>2</sub> CuO <sub>4</sub> (44)                 | 8.8                         | 1.3                       | 3.5                            | 6.0                         | 4.5            | 6.1         | 0.98  | 140 (48)                    | 1.2       | 3.7            | 0.38  |
| La <sub>2</sub> CuO <sub>4</sub> (46)                 | 9.61                        | 1.37                      | 3.7                            | 6.1                         | 4.6            | 6.2         | 0.79  | 140 (48)                    | 1.2       | 3.9            | 0.36  |
| Hg1201(46)  | 8.84                        | 1.26                      | 2.42                           | 5.3                         | 4.4            | 5.4         | 3.78  | 135 (65)                    | 0.9       | 2.6            | 0.75  |
| Bi2212(67)  | 8.5                         | 1.13                      | 3.2                            | 4.1                         | 3.5            | 4.1         | 0.06  | 161 (66)                    | 1.1       | 3.5            | 0.06  |
| Spectroscopy  |                             |                           |                                |                             |                |             |       |                             |           |                |       |
| CuO(38,54)  | 7.7                         | 1.55                      | 2.5                            | 5                           | 7.6            | 5.4         | 25.9  | 91 (68*)                    | 0.8       | 2.6            | 1.72  |
| Sr <sub>2</sub> CuO <sub>3</sub> (51,52)              | 8.8                         | 1.45                      | 2.5                            | 4.4                         | 4.4            | 4.6         | 3.62  | 241 (60)                    | 1.1       | 2.8            | 0.96  |
| Sr <sub>2</sub> CuO <sub>2</sub> Cl <sub>2</sub> (53) | 8.8                         | 1.5                       | 3.5                            | 4.4                         | 6.0            | 4.6         | 6.45  | 130(49,50)                  | 1.1       | 3.7            | 1.04  |
| La <sub>2</sub> CuO <sub>4</sub> (54,55)              | 7.0                         | 1.5                       | 3.5                            | 6.0                         | 6.0            | 6.2         | 6.49  | 140 (48)                    | 1.13      | 3.7            | 1.0   |
| Nd <sub>2</sub> CuO <sub>4</sub> (56)                 | 8.0                         | 1.1                       | 3.0                            | 4.1                         | 3.6            | 4.1         | 0.41  | 133 (61)                    | 1.0       | 3.2            | 0.21  |
| Pr <sub>2</sub> CuO <sub>4</sub> (56)                 | 8.0                         | 1.1                       | 3.0                            | 4.1                         | 3.8            | 4.2         | 0.62  | 121 (61)                    | 1.0       | 3.2            | 0.26  |
| YBCO(37,39)   | 7.0                         | 1.2                       | 1.5                            | 5.0                         | 4.4            | 5.2         | 8.2   | 125 (62)                    | 0.7       | 1.7            | 0.99  |
| Bi2212(59)  | 7.7                         | 1.5                       | 3.5                            | 6.0                         | 5.6            | 6.1         | 4.3   | 161 (66)                    | 1.2       | 3.7            | 0.88  |
| RIXS  |                             |                           |                                |                             |                |             |       |                             |           |                |       |
| Bi2201(65)  | 10.2                        | 1.35                      | 3.9                            | 5.9                         | 4.5            | 5.9         | 0.34  | 153                         | 1.3       | 4.1            | 0.22  |

(\*For CuO, the dominant exchange interaction  $J$  which couples antiferromagnetically is the one along the  $[10\bar{1}]$  chain direction and considered here, while the nearest neighbor spins exhibit a weak ferromagnetic coupling (ref. 68).)

TABLE II: Renormalized Electronic parameters for cuprates in the one-band Hubbard model along with the ground state singlet weights  $c_{21}$  (between the two Cu sites) and  $c_{13}$  (between the Cu and O site).

| Compound  | $\tilde{U}$<br>eV | $\tilde{t}$<br>eV | $\tilde{U}/\tilde{t}$ | $J$<br>meV | $\tilde{U}$<br>eV | $\tilde{t}$<br>eV | $\tilde{U}/\tilde{t}$ | $c_{21}$ | $c_{13}$ |
|---|-------------------|-------------------|-----------------------|------------|-------------------|-------------------|-----------------------|----------|----------|
| Theory  |                   |                   |                       |            |                   |                   |                       |          |          |
| La <sub>2</sub> CuO <sub>4</sub> (42)                 | 4.38              | 0.39              | 11.18                 | 140        | 3.68              | 0.36              | 10.26                 | 0.65     | 0.2      |
| La <sub>2</sub> CuO <sub>4</sub> (43)                 | 4.03              | 0.37              | 10.73                 | 140        | 3.7               | 0.36              | 10.28                 | 0.65     | 0.2      |
| La <sub>2</sub> CuO <sub>4</sub> (44)                 | 4.05              | 0.38              | 10.76                 | 140        | 3.81              | 0.37              | 10.42                 | 0.64     | 0.2      |
| La <sub>2</sub> CuO <sub>4</sub> (46)                 | 4.27              | 0.41              | 10.43                 | 140        | 4.05              | 0.4               | 10.16                 | 0.64     | 0.2      |
| Hg1201(46)  | 3.93              | 0.36              | 10.79                 | 135        | 3.3               | 0.33              | 9.89                  | 0.63     | 0.21     |
| Bi2212(66)  | 3.35              | 0.37              | 9.13                  | 161        | 3.34              | 0.37              | 9.11                  | 0.64     | 0.2      |
| Spectroscopy  |                   |                   |                       |            |                   |                   |                       |          |          |
| CuO(38,54)  | 4.39              | 0.32              | 13.87                 | 91         | 3.09              | 0.27              | 11.62                 | 0.64     | 0.2      |
| Sr <sub>2</sub> CuO <sub>3</sub> (51,52)              | 3.79              | 0.48              | 7.94                  | 241        | 3.17              | 0.44              | 7.25                  | 0.62     | 0.23     |
| Sr <sub>2</sub> CuO <sub>2</sub> Cl <sub>2</sub> (53) | 4.28              | 0.37              | 11.47                 | 130        | 3.53              | 0.34              | 10.42                 | 0.65     | 0.19     |
| La <sub>2</sub> CuO <sub>4</sub> (54,55)              | 3.96              | 0.37              | 10.64                 | 140        | 3.42              | 0.34              | 9.89                  | 0.64     | 0.2      |
| Nd <sub>2</sub> CuO <sub>4</sub> (56)                 | 3.33              | 0.33              | 10.01                 | 133        | 3.17              | 0.32              | 9.75                  | 0.64     | 0.2      |
| Pr <sub>2</sub> CuO <sub>4</sub> (56)                 | 3.38              | 0.32              | 10.58                 | 121        | 3.16              | 0.31              | 10.23                 | 0.64     | 0.2      |
| YBCO(37,39)   | 3.49              | 0.33              | 10.56                 | 125        | 2.61              | 0.29              | 9.14                  | 0.62     | 0.23     |
| Bi2212(59)  | 4.07              | 0.4               | 10.05                 | 161        | 3.59              | 0.38              | 9.44                  | 0.64     | 0.2      |
| RIXS  |                   |                   |                       |            |                   |                   |                       |          |          |
| Bi2201(65)  | 4.31              | 0.41              | 10.61                 | 153        | 4.18              | 0.4               | 10.45                 | 0.65     | 0.2      |

For example, it was shown that neutron scattering of La<sub>2</sub>CuO<sub>4</sub> provided a dominant nearest neighbor (NN) hopping  $t = 0.33$  eV and an effective  $U/t = 8.8$  eV with  $U = 2.9$  eV, but also showed that in addition to the NN

exchange  $J = 138$  meV, it was important to include ring exchange  $J_c = 38$  meV, while  $J' = J'' = 2$  meV were small<sup>48</sup>. Similarly, for Sr<sub>2</sub>CuO<sub>2</sub>Cl<sub>2</sub>, the  $t - t' - t'' - J$  model showed  $t = 0.35$  eV, while  $t' = 0.12$  eV, and

TABLE III: Examples of one-band model electronic parameters estimated independently from magnon dispersion in neutron scattering, band dispersion in angle-resolved photoemission spectroscopy(ARPES) and from *ab initio* theory.

| Compound<br>(ref. no)                                    | $\tilde{U}$<br>eV | $\tilde{t}$<br>eV | $\tilde{U}/\tilde{t}$ | Method                  |
|--|-------------------|-------------------|-----------------------|-------------------------|
| La <sub>2</sub> CuO <sub>4</sub> (48)                    | 2.9               | 0.33              | 8.8                   | Neutron scattering      |
| Sr <sub>2</sub> CuO <sub>2</sub> Cl <sub>2</sub> (49,50) | 3.5               | 0.35              | 10.0                  | ARPES                   |
| La <sub>2</sub> CuO <sub>4</sub> (46)                    | 5.0               | 0.48              | 10.4                  | <i>ab initio</i> theory |
| Hg1201 (46)  | 4.4               | 0.46              | 9.5                   | <i>ab initio</i> theory |

$t'' = 0.08$  eV, and with a  $J = 0.14$  eV, it implied an effective  $U/t = 10$  with  $U = 3.5$  eV<sup>50</sup>. For CuO, a recent study showed that a linear spin-wave model for a Heisenberg antiferromagnet provided a good description of the neutron scattering results<sup>68</sup>. The relevant exchange constants could be accurately determined and showed that the dominant exchange interaction  $J = 91$  meV, which coupled antiferromagnetically along the [101] chain direction, while the nearest neighbor interchain interactions were very weak ( $J_{ac} = 3.9$  meV and  $J_b = 0.39$  meV) and coupled ferromagnetically<sup>68</sup>.

Given this dichotomy between the theoretical one-band versus the three-band models, and the corresponding experimental high-energy spectroscopies versus the low-energy magnon and band dispersion measurements, we felt it important to address a possible connection between them. In this study, we have found this connection by using the nearest neighbor Heisenberg exchange interaction  $J$  obtained from neutron scattering and RIXS experiments<sup>48,60–66,68</sup> as a bridge to connect electronic parameters known from experiment (high-energy spectroscopy, RIXS, neutron scattering) and theory in the one-band and three-band Hubbard models. The results show that the three-band Hubbard model parameters can be recast as a one-band Hubbard model in terms of a renormalized  $\tilde{U}$  and  $\tilde{t}$  with  $J = 4\tilde{t}^2/\tilde{U}$ .

We now summarize our main results. We calculate  $J$ , the strength of the Heisenberg coupling between Cu moments in a Cu<sub>2</sub>O cluster, using the downfolding method discussed by Koch<sup>41</sup>. For several compounds neutron scattering data for  $J$  and spectroscopic data for  $U_d$ ,  $U_p$ ,  $\Delta$  and  $t$  are available. Directly using the spectroscopic parameter values in the downfolding expression for  $J$  leads to deviations from the experimental  $J$  values. We therefore use two estimation procedures, referred to as Optimization-1 and Optimization-2 in the following, to modify a subset (different in the two procedures) of the spectroscopic data, so that there is a good agreement with experimental  $J$  values using the procedure described in Sec. II. We identify effective parameters  $\tilde{t}$  and  $\tilde{U}$  so that the downfolding expression for  $J$  becomes equal to  $4\tilde{t}^2/\tilde{U}$ . The estimated values of  $\tilde{t}$  and  $\tilde{U}$  are found to be consistently smaller than  $t$  and  $U_d$  in all cases, but lead to a larger  $\tilde{U}/\tilde{t}$  in the one-band case compared to

the  $U_d/t$  of the three-band case, in good agreement with theoretical estimates reported in the literature. The results indicate that stronger effective correlations, arising from a combination of  $U_d$ ,  $U_p$  and  $\Delta$ , are hidden in the effective one-band Hubbard model. The study provides a consistent method to connect electronic parameters obtained from spectroscopy and the three-band model on the one hand, with values obtained from neutron scattering, ARPES measurements and the effective one-band Hubbard model on the other.

## II. CALCULATIONS

We consider a Cu<sub>2</sub>O cluster with site labels  $i = 1, 2$  (for Cu(1) and Cu(2) atoms) and  $i = 3$  (for the O atom). The cluster hamiltonian is

$$\hat{H} = \frac{\Delta}{2}(n_3 - n_1 - n_2) - t \sum_{i\sigma} (d_{i\sigma}^\dagger p_\sigma + h.c.) + U_d(n_{1\uparrow}n_{1\downarrow} + n_{2\uparrow}n_{2\downarrow}) + U_p n_{3\uparrow}n_{3\downarrow}, \quad (1)$$

where  $n_{i\sigma}^d = d_{i\sigma}^\dagger d_{i\sigma}$  ( $i = 1, 2$ ),  $n_{3\sigma} = p_\sigma^\dagger p_\sigma$  and  $n_i = n_{i\uparrow} + n_{i\downarrow}$ . Here,  $d_{i\sigma}^\dagger$  creates a hole with a  $z$  component of spin  $\sigma = \pm 1/2$  in the Cu  $d$  orbital at site  $i$  ( $= 1, 2$ ), and  $p_\sigma^\dagger$  creates a hole with a  $z$  component of spin  $\sigma = \pm 1/2$  in the O  $p$  orbital at the site located in between the two Cu sites.  $\Delta$  is the charge-transfer energy; the parameters  $U_p$  and  $U_d$  are onsite repulsion energies at the O and Cu sites, respectively; and finally  $t$  is the strength of hopping between neighboring O and Cu sites.

In this work, we consider a filling fraction corresponding to undoped cuprates, in which the outermost  $p$  orbital on the O site is filled with two electrons (i.e. empty in the hole picture), and the outermost  $d$  orbital on the Cu site has one electron (i.e. one hole), in the absence of hopping. For our cluster with three atoms, this corresponds to a total occupancy of four electrons, or two holes. The two holes can be selected in three ways: both with  $\sigma = -1/2$  (the ferromagnetic down case), both with  $\sigma = 1/2$  (the ferromagnetic up case), and finally, one hole with  $\sigma = 1/2$  and another with  $\sigma = -1/2$  (the antiferromagnetic case).

We will consider only the antiferromagnetic case henceforth. In this case, there are 9 basis states

$|i, j\rangle$ ,  $i, j = 1, 2, 3$ . In state  $|i, j\rangle$ ,  $i$  and  $j$  are the Cu ( $i, j = 1, 2$ ) or O ( $i, j = 3$ ) sites with up and down holes, respectively. In the basis  $\{|1, 2\rangle, |2, 1\rangle, |1, 3\rangle, |3, 1\rangle, |2, 3\rangle, |3, 2\rangle, |1, 1\rangle, |2, 2\rangle, |3, 3\rangle\}$ , the hamiltonian (1) becomes a  $9 \times 9$  matrix

$$H = \begin{bmatrix} H_{00} & H_{01} & H_{02} \\ H_{10} & H_{11} & H_{12} \\ H_{20} & H_{21} & H_{22} \end{bmatrix}, \quad (2)$$

in which the blocks are

$$H_{00} = -\Delta \begin{bmatrix} 1 & 0 \\ 0 & 1 \end{bmatrix}, \quad H_{01} = \begin{bmatrix} t & 0 & 0 & -t \\ 0 & t & -t & 0 \end{bmatrix},$$

$$H_{02} = O_{2 \times 3}, \quad H_{11} = O_{4 \times 4}, \quad H_{12} = \begin{bmatrix} t & 0 & t \\ -t & 0 & -t \\ 0 & t & t \\ 0 & -t & -t \end{bmatrix},$$

$$\text{and } H_{22} = \begin{bmatrix} U_d - \Delta & 0 & 0 \\ 0 & U_d - \Delta & 0 \\ 0 & 0 & U_p + \Delta \end{bmatrix}. \quad (3)$$

In the above,  $O_{m \times n}$  denotes an  $m \times n$  matrix of zeros. We calculate the Heisenberg antiferromagnetic coupling  $J$  between the Cu(1) and Cu(2) spins based on the down-folding fourth-order perturbation method described in Koch<sup>41</sup> and Zurek<sup>69</sup>. Accordingly, the effective hamiltonian is

$$\begin{aligned} \tilde{H} &= H_{00} + H_{01}(\epsilon - (H_{11} + H_{12}(\epsilon - H_{22})^{-1}H_{21})^{-1})^{-1}. \\ &\approx H_{00} + H_{01}(\epsilon - H_{11})^{-1}H_{10} + \\ &\quad H_{01}(\epsilon - H_{11})^{-1}H_{12}(\epsilon - H_{22})^{-1}H_{21}(\epsilon - H_{11})^{-1}H_{10} \end{aligned} \quad (4)$$

where we have used the approximation  $(A + B)^{-1} \approx A^{-1}(1 - BA^{-1})$ . We now take  $\epsilon = -\Delta$  and perform the matrix products above. The result is

$$\tilde{H} \approx -\frac{2t^2}{\Delta} \begin{bmatrix} 1 & 0 \\ 0 & 1 \end{bmatrix} - \frac{J}{2} \begin{bmatrix} 1 & -1 \\ -1 & 1 \end{bmatrix} \quad (5)$$

where the Heisenberg coupling is

$$J = 4 \frac{t^4}{\Delta^2} \left[ \frac{1}{U_d} + \frac{2}{2\Delta + U_p} \right]. \quad (6)$$

The result we have obtained for  $J$  using the down-folding approximation is the same as that obtained by Khomskii<sup>40</sup> using a fourth-order perturbation theory. If we now define  $\tilde{t}$  and  $\tilde{U}$  using

$$\tilde{t} = \frac{t^2}{\Delta}, \quad \frac{1}{\tilde{U}} = \frac{1}{U_d} + \frac{1}{\Delta + U_p/2} \quad (7)$$

then  $J = 4\tilde{t}^2/\tilde{U}$ . This is the expression for  $J$  we would get if we used a one-band Hubbard model with a hopping strength  $\tilde{t}$  and an on-site repulsion  $\tilde{U} \gg \tilde{t}$ , using second-order perturbation theory. In this sense, we consider  $\tilde{U}$

and  $\tilde{t}$  as the parameters of an effective one-band Hodel model corresponding to the model in (1).

We find that using the spectroscopic values on the right-hand side and the experimental  $J$  values on the left-hand side of equation (6) does not satisfy the equation with sufficient accuracy. We therefore modify, in an optimal manner described below, a subset of the spectroscopic parameter values so that the agreement is good.

We now describe two such simple optimization procedures. We define the parameter  $R = \tilde{U}/\tilde{t}$  to obtain the parametric forms  $\tilde{t} = RJ/4$ ,  $\tilde{U} = R^2J/4$  for the effective parameters. These are the expressions that we use below for  $\tilde{t}$ ,  $\tilde{U}$ .

In the Optimization-1 procedure, we modify  $(\Delta, U_p)$ . We solve the relations (7) to obtain  $\Delta_1(R) = t^2/\tilde{t}$  and  $U_p(R)/2 = U_d\tilde{U}/(U_d - \tilde{U}) - \Delta_1(R)$ . We then minimize a cost function  $f_1(R) = (\Delta_1(R) - \bar{\Delta})^2 + (U_p(R) - \bar{U}_p)^2$  with respect to  $R$  to obtain the minimum  $R^*$ , using the spectroscopic values for  $t$ ,  $U_d$ ,  $\bar{\Delta}$ ,  $\bar{U}_p$  and neutron scattering values for  $J$ . This estimates  $\Delta(R^*)$ ,  $U_p(R^*)$ ,  $\tilde{U}(R^*)$ , and  $\tilde{t}(R^*)$ .

In the Optimization-2 procedure, we modify  $(\Delta, t)$ . We solve the relations (7) to obtain  $t(R)^2 = \Delta_2(R)\tilde{t}$  and  $\Delta_2(R) = U_d\tilde{U}/(U_d - \tilde{U}) - U_p/2$ . We then minimize a cost function  $f_2(R) = (\Delta_2(R) - \bar{\Delta})^2 + |(t(R)^2 - \bar{t}^2)|$  with respect to  $R$  to obtain the minimum  $R^*$ , using the spectroscopic values for  $\bar{t}$ ,  $U_d$ ,  $\bar{\Delta}$ ,  $U_p$  and neutron scattering values for  $J$ . This estimates  $\Delta(R^*)$ ,  $t(R^*)$ ,  $\tilde{U}(R^*)$ , and  $\tilde{t}(R^*)$ .

### III. RESULTS AND DISCUSSION

The results are summarized in Table 1 and Table 2 for a variety of CuO-based materials. Table 1 presents our estimates of the spectroscopic, three-band, model parameters, while Table 2 presents our estimates of effective one-band parameters. Both tables contain results of the two optimization procedures that we discussed above.

In Table 1, the columns 5-7 present results of Optimization-1 procedure: these are values of  $\Delta$ ,  $U_p$  and  $f_1$ ; the columns 9-11 present results of Optimization-2 procedure: these are values of  $t$ ,  $\Delta$  and  $f_2$ . We can see from the cost function values that Optimization-2 is better than Optimization-1; this is also reflected in the greater closeness of  $(t, \Delta)$  estimates to measured values than that of  $(\Delta, U_p)$  estimates to measured values. Considering that  $J$  depends on  $t^4$  in equation (6), it can be seen that a smaller spread in  $t$  across compounds provides a better description of parameter values; further since  $\Delta$  and  $t$  are intimately related through the first relation in equation (7), it makes sense to optimize with respect to these two parameters as done in Optimization-2. This has the result of reducing the spread in estimated  $t$  values compared with reported spectroscopic  $t$  values. This also improves the estimates of  $\Delta$  compared with those in Optimization-1. For these reasons, we can understand that Optimization-2 is better than not

only Optimization-1, but also other possible optimization choices, namely  $(\Delta, U_d)$ ,  $(t, U_p)$  and  $(t, U_d)$ . We therefore do not present the results of these latter procedures.

Since  $R = \tilde{U}/\tilde{t} \sim 10$  in most cases (see columns 4 and 8 in Table 2), we can see that it makes sense to treat  $\tilde{U}$ ,  $\tilde{t}$  as effective one-band parameters, as noted before. We observe that  $R \sim 10$  not only in cases where spectroscopic three-band parameter values are reported, but also for theoretical as well as RIXS three-band numbers (see Table 2).

Secondly,  $\tilde{U}$  is roughly half of  $U_d$  in almost all cases. This shows that the effective model is not a simple Cu  $d$ -band model, but possibly a more hybrid one involving Cu- $d$  and O- $(p_x, p_y)$  orbitals. To understand this better, we have looked at the nature of the ground state obtained by exactly diagonalizing the cluster hamiltonian (1) for each compound in Table 1 using our Optimization-2 estimates of the three-band parameters. The ground state we obtain,  $|G\rangle = \sum_{ij} c_{ij}|i, j\rangle$ , always has the property  $c_{12} = -c_{21}, c_{13} = -c_{31} = c_{23} = -c_{32}, c_{11} = c_{22}$  by symmetry, which shows that it is a singlet of Cu and O orbitals. We can thus completely characterize the ground state with the two distinct singlet weights  $c_{21}$  and  $c_{13}$  and the two distinct hole double-occupancy weights  $c_{11}$  and  $c_{33}$ . Since our focus is primarily on the singlet nature of  $|G\rangle$ , we present  $c_{21}$  and  $c_{13}$  in Table 2 (see columns 9 and 10). The singlet weights of the Cu-Cu and Cu-O sectors clearly show that the ground state is a hybrid singlet of Cu- $d$  and O- $(p_x, p_y)$  orbitals, or is in other words, a Zhang-Rice singlet (ZRS). The effective interaction  $\tilde{U}$  is thus not between purely Cu- $d$  holes, but represents the hybrid Zhang-Rice singlets, and is therefore significantly smaller than  $U_d$ . However, it must also be noted from Table 1 and Table 2 that  $\tilde{U}/\tilde{t} \simeq 10$ , satisfying the strong correlation condition in the effective one-band model. In Table 3, we list a few examples of one-band model electronic parameters estimated independently, from magnon dispersion in neutron scattering, band dispersion in angle-resolved photoemission spectroscopy (ARPES) and from ab-initio theory. It is clear that the values of  $\tilde{U}/\tilde{t}$  in all the cases are close to the values in Table 2 and validates our analysis.

As it is well-known that the Heisenberg model is a good approximation of Eq. (1) for small  $t$ , in Fig.1, we present a comparison of  $J$  obtained from the downfolding approximation with  $E_2 - E_1$ , the difference in energy between the ground and first excited states from our exact diagonalization calculation. The plot shows  $J$  and  $E_2 - E_1$  as a function of  $t$ , varied from 0 to 1.6 eV, for  $U_p = 1, 3$  and 5 eV; we have fixed the values  $U_d = 8$  eV and  $\Delta = 3.3$  eV (=average  $\Delta$  of values obtained by optimization 2 shown in Table 1) in these plots. We can see that there is good agreement between  $J$  and  $E_2 - E_1$  at low values of  $t$ . In order to explore this carefully, in the inset we plot the ratio of  $(E_2 - E_1)/J$  which confirms that the downfolding approximation for  $J$  holds for low values of  $t$ . As  $t \rightarrow 0$ , the ratio is 1 and decreases on increasing  $t$ . The ratio is 0.83 at  $t = 0.7$  eV, and it becomes 0.62 at  $t =$

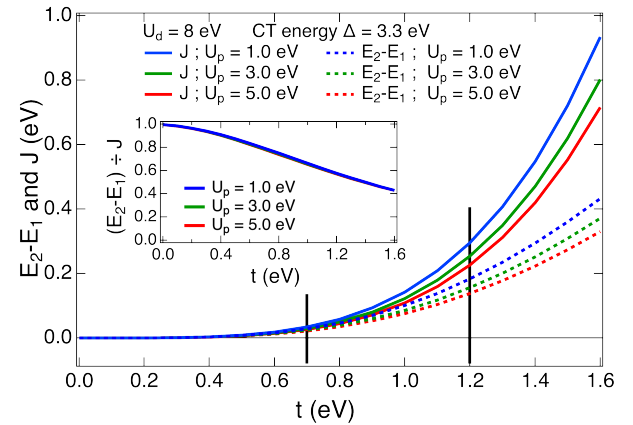


FIG. 1: Comparison of the exchange interaction  $J$  (calculated using eqn. 6) and  $E_2 - E_1$ , the difference in energy between the ground and first excited states from the exact diagonalization, plotted as a function of hopping,  $t$ . The inset shows a plot of the ratio  $(E_2 - E_1)/J$  which confirms that the downfolding approximation for  $J$  holds for small  $t$ .

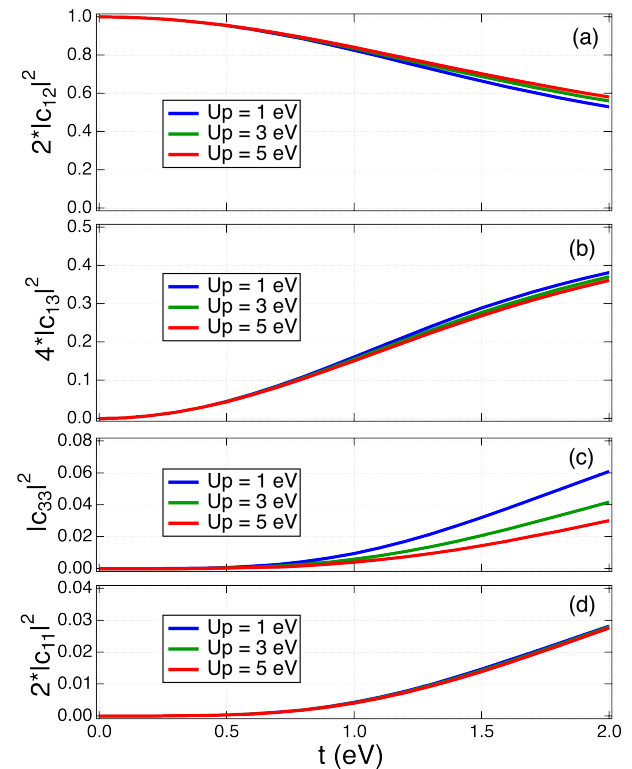


FIG. 2: (a-d) Plots of various calculated total weights  $|c_{ij}|^2$  as a function of  $t$ , for the same parameter settings as in Fig.1. (a) shows the total Cu(1)-Cu(2) singlet weight  $2|c_{12}|^2$ . (b) shows the total Cu(1)-O(3) singlet weight  $4|c_{13}|^2$ . (c) and (d) show the on-site double occupancy weights  $|2c_{11}|^2$  (total for the Cu(1) and Cu(2) sites) and  $|c_{33}|^2$  for the O(3) site.

1.2 eV, ( this range of  $t$  spans the values we find for the cuprates in Table 1 ; black vertical lines in Fig.1). Since  $J \sim t^4$ , it increases rapidly for increasing  $t$  eV, while the increase in  $E_2 - E_1$  can be seen to be slower. For values of  $t \simeq 0.7 - 1.2$  eV describing the cuprates, we believe we can still justify the use of the downfolding expression to understand the low-lying excitations in these cases. Finally in Fig. 2(a-d) we present plots of various  $|c_{ij}|^2$  as a function of  $t$ , for the same parameter settings as in Fig.1. Fig. 2(a) shows that the pure Cu(1)-Cu(2) singlet weight  $2|c_{12}|^2 \sim 1$  obtained for  $t = 0$  systematically reduces in weight on increasing  $t$ . Simultaneously, the total Cu(1)-O(3) singlet weight  $4|c_{13}|^2$  increases systematically on increasing  $t$ , indicating the role of Cu-O hybridization in forming the ZRS state for the cuprates. Thus, the O- $p$  orbital plays an increasingly important role on increasing  $t$  to  $\sim 1$  eV, typical of the cuprates. Further, the on-site double occupancy weights  $|c_{ii}|^2$ ,  $i = 1-3$ , are quite small (Fig. 2(c,d)). However, on increasing  $U_p$  from 1 to 5 eV, while there is hardly any change in the total double occupancy weight  $2|c_{11}|^2$  on the Cu sites, the double occupancy weight  $|c_{33}|^2$  on the O site gets suppressed to nearly half its value for  $t > 1$  eV. This behavior of the O site double occupancy is closely related to the reduction of  $J$  by  $U_p$  according to Eq. (6), and is also seen in Fig.1. Thus,  $U_p$  plays an important role in tuning the value of  $J$ , which is considered to be one of the most important parameters to achieve high-temperature superconductivity exhibited by the family of cuprates<sup>1,48,60-66,70-73</sup>.

#### IV. CONCLUDING REMARKS

In this work, we have presented a data analysis of spectroscopic parameters and neutron-scattering parameters for a variety of cuprates based on a theoretical relationship between the parameters of a three-band model and an effective one-band Heisenberg antiferromagnetic coupling, using a cluster-model calculation. We have also performed an exact diagonalization of the cluster hamiltonian to understand the nature of the ground state.

Our analysis shows  $\tilde{U} < U_d$  always. In addition to agreeing with estimates of  $\tilde{U}$  from the one-band model

applied to neutron scattering or ARPES experiments, this inequality is a direct consequence of equation (7).

$U_p$  is significant in magnitude, both in measurements and in our estimates, far from being too small! Surprisingly,  $U_p$  tends to be ignored in many studies on cuprates, but we believe that this needs to be revisited. Indeed, the second relation in equation (7) shows that the effective interaction  $\tilde{U}$  is enhanced by  $U_p$  and  $\Delta$ .

The ground-state singlet weights from our exact diagonalization show the importance of O moments and ZRS in the effective description. We also observe that the singlet weights change very little across the family of compounds, in spite of a variation in the three-band spectroscopic parameters that are used to calculate them. This holds for the ratio  $\tilde{U}/t$  as well.

$\tilde{U}/t \sim U_d/t \sim 10$  in all cases, pointing to the effective one-band model being strongly correlated.

As to the spectroscopic values of the three-band parameters, it is generally believed that  $\Delta$  and  $t$  measurements are less reliable than those of  $U_d$  and  $U_p$ . Our estimation procedure Optimization-2 attempts to offer a reasonable description of the spectroscopic and neutron-scattering data by reducing the spread in the values of  $\Delta$  and  $t$  across the family of cuprates.

In conclusion, we have performed a perturbative and exact diagonalization study of a model of a Cu<sub>2</sub>O cluster that connects electronic parameters obtained from spectroscopy and the three-band model with values of  $J$  obtained from scattering, band dispersion measurements and the effective one-band Hubbard model.

#### V. ACKNOWLEDGMENTS

AF thanks JSPS KAKENHI (Grant Numbers JP19K03741 and JP22K03535) and the “Program for Promoting Researches on the Supercomputer Fugaku” (Basic Science for Emergence and Functionality in Quantum Matter, JPMXP1020200104) from MEXT. AC thanks the National Science and Technology Council (NSTC) of the Republic of China, Taiwan for financially supporting this research under Contract No. MOST 111-2112-M-213-031.

<sup>1</sup> B. Keimer, S. A. Kivelson, M. R. Norman, S. Uchida and J. Zaanen, *Nature* 518, 179 (2015).

<sup>2</sup> J. G. Bednorz and K. A. Mueller, *Z. fur Physik B* 64, 189 (1986).

<sup>3</sup> P. W. Anderson, in *Frontiers and Borderlines in Many-Particle Physics*, edited by J. R. Schrieffer and R. A. Broglia (NorthHolland, Amsterdam, 1988).

<sup>4</sup> F. C. Zhang and T. M. Rice, *Phys. Rev. B* 37, 3759 (1988).

<sup>5</sup> G. Baskaran, Z. Zou, P.W. Anderson, *Solid State Comm.*, 63, 973 (1987).

<sup>6</sup> C. M. Varma, S. Schmitt-Rink, and E. Abrahams, *Solid*

*State Commun.* 62, 681 (1987).

<sup>7</sup> V. J. Emery, *Phys. Rev. Lett.* 58, 2794 (1987).

<sup>8</sup> J. Spalek and A. M. Oles, *Physica B* 86-88, 375 (1977).

<sup>9</sup> H. J. Schulz, *Superconductivity and Antiferromagnetism in the Two-Dimensional Hubbard Model: Scaling Theory* *Europhysics Letters*, EPL 4, 609 (1987).

<sup>10</sup> C. M. Varma, P. B. Littlewood, S. Schmitt-Rink, E. Abrahams, and A. E. Ruckenstein, *Phenomenology of the normal state of Cu-O high-temperature superconductors*, *Phys. Rev. Lett.* 63, 1996 (1989).

<sup>11</sup> Daniel F. Agterberg, J. C. Seamus Davis, Stephen D. Ed-

kins, Eduardo Fradkin, Dale J. Van Harlingen, Steven A. Kivelson, Patrick A. Lee, Leo Radzihovsky, John M. Tranquada, Yuxuan Wang, The Physics of Pair Density Waves, Annual Review of Condensed Matter Physics 11, 231 (2020).

<sup>12</sup> A.R. Bishop, R. M. Martin, K.A. Muller, and Z. Tesanovic, Z. Phys. B 76, 413 (1989).

<sup>13</sup> J. Rossat-Mignod, L. P. Regnault, C. Vettier, P. Bourges, P. Burlet, J. Bossy, J. Y. Henry, and G. Lapertot, Physica C 185-189, 86 (1991).

<sup>14</sup> M. Eschrig, Adv. Phys. 55, 47 (2006).

<sup>15</sup> M. Le Tacon, G. Ghiringhelli, J. Chaloupka, M. Moretti Sala, V. Hinkov, M. W. Haverkort, M. Minola, M. Bakr, K. J. Zhou, S. Blanco-Canosa, C. Monney, Y. T. Song, G. L. Sun, C. T. Lin, G. M. De Luca, M. Salluzzo, G. Khaliullin, T. Schmitt, L. Braicovich, and B. Keimer, Nat. Phys. 7, 725 (2011).

<sup>16</sup> J. M. Tranquada, B. J. Sternlieb, J. D. Axe, Y. Nakamura and S. Uchida, Nature 375, 561 (1995).

<sup>17</sup> T. Wu, H. Mayaffre, S. Kramer, M. Horvatic, C. Berthier, W. N. Hardy, R. Liang, D. A. Bonn and M.-H. Julien, Nature 477, 191 (2011).

<sup>18</sup> G. Ghiringhelli, M. Le Tacon, M. Minola, S. Blanco-Canosa, C. Mazzoli, N. B. Brookes, G. M. De Luca, A. Frano, D. G. Hawthorn, F. He, T. Loew, M. Moretti Sala, D. C. Peets, M. Salluzzo, E. Schierle, R. Sutarto, G. A. Sawatzky, E. Weschke, B. Keimer, L. Braicovich, Science 337, 821 (2012).

<sup>19</sup> J. Chang, E. Blackburn, A. T. Holmes, N. B. Christensen, J. Larsen, J. Mesot, Ruixing Liang, D. A. Bonn, W. N. Hardy, A. Watenphul, M. v. Zimmermann, E. M. Forgan and S. M. Hayden, Nature Physics 8, 871 (2012).

<sup>20</sup> M. Le Tacon, A. Bosak, S. M. Souliou, G. Dellea, T. Loew, R. Heid, K-P. Bohnen, G. Ghiringhelli, M. Krisch and B. Keimer, Nature Physics 10, 52 (2014).

<sup>21</sup> W. Tabis, Y. Li, M. Le Tacon, L. Braicovich, A. Kreyssig, M. Minola, G. Dellea, E. Weschke, M. J. Veit, M. Raramanoglu, A. I. Goldman, T. Schmitt, G. Ghiringhelli, N. Barisic, M. K. Chan, C. J. Dorow, G. Yu, X. Zhao, B. Keimer and M. Greven, Nat. Commun. 5:5875 doi: 10.1038/ncomms6875 (2014).

<sup>22</sup> S. Gerber, H. Jang, H. Nojiri, S. Matsuzawa, H. Yasumura, D. A. Bonn, R. Liang, W. N. Hardy, Z. Islam, A. Mehta, S. Song, M. Sikorski, D. Stefanescu, Y. Feng, S. A. Kivelson, T. P. Devereaux, Z.-X. Shen, C.-C. Kao, W.-S. Lee, D. Zhu, and J.-S. Lee, Science 350, 949 (2015).

<sup>23</sup> M.-H. Julien, P. Carretta, M. Horvatic, C. Berthier, Y. Berthier, P. Segransan, A. Carrington, and D. Colson, Phys. Rev. Lett. 76, 4238(1996).

<sup>24</sup> W. S. Lee, J. J. Lee, E. A. Nowadnick, S. Gerber, W. Tabis, S. W. Huang, V. N. Strocov, E. M. Motoyama, G. Yu, B. Moritz, H. Y. Huang, R. P. Wang, Y. B. Huang, W. B. Wu, C. T. Chen, D. J. Huang, M. Greven, T. Schmitt, Z. X. Shen and T. P. Devereaux, Nature Physics 10, 883 (2014).

<sup>25</sup> M. K. Chan, C. J. Dorow, L. Mangin-Thro, Y. Tang, Y. Ge, M. J. Veit, G. Yu, X. Zhao, A. D. Christianson, J. T. Park, Y. Sidis, P. Steffens, D. L. Abernathy, P. Bourges and M. Greven, Nature Communications 7, 10819 (2016).

<sup>26</sup> M. I. Salkola, V. J. Emery, and S. A. Kivelson, Phys. Rev. Lett. 77, 155 (1996).

<sup>27</sup> A. Lanzara, P. V. Bogdanov, X. J. Zhou, S. A. Kellar, D. L. Feng, E. D. Lu, T. Yoshida, H. Eisaki, A. Fujimori, K. Kishio, J.-I. Shimoyama, T. Noda, S. Uchida, Z. Hussain and Z.-X. Shen, Nature 412, 510 (2001).

<sup>28</sup> J. Zaanen, G. A. Sawatzky and J. W. Allen, Phys. Rev. Lett. 55, 418 (1985).

<sup>29</sup> C. T. Chen, L. H. Tjeng, J. Kwo, H. L. Kao, P. Rudolf, F. Sette, and R. M. Fleming, Phys. Rev. Lett. 68, 2543 (1992).

<sup>30</sup> N. B. Brookes, G. Ghiringhelli, O. Tjernberg, L. H. Tjeng, T. Mizokawa, T.W. Li and A. A. Menovsky, Phys. Rev. Lett. 87, 237003 (2001).

<sup>31</sup> N.B. Brookes, G. Ghiringhelli, A.-M. Charvet, A. Fujimori, T. Kakeshita, H. Eisaki, S. Uchida, and T. Mizokawa, Phys. Rev. Lett. 115, 027002 (2015).

<sup>32</sup> M Cini, Solid State Communications 20, 605 (1976); 24, 681-684 (1977); Phys. Rev. B 17, 2788 (1978).

<sup>33</sup> G. A. Sawatzky, Phys. Rev. Lett. 39, 504 (1977).

<sup>34</sup> A. Fujimori, E. Takayama-Muromachi, Y. Uchida, and B. Okai, Phys. Rev. B 35, 8814(R) (1987).

<sup>35</sup> Z.-X. Shen, J. W. Allen, J. J. Yeh, J. -S. Kang, W. Ellis, W. Spicer, I. Lindau, M. B. Maple, Y. D. Dalichaouch, M. S. Torikachvili, J. Z. Sun, and T. H. Geballe, Phys. Rev. B 36, 8414 (1987).

<sup>36</sup> A. Balzarotti, M. De Crescenzi, N. Motta, F. Patella, and A. Sgarlata, Phys. Rev. B 38, 6461 (1988).

<sup>37</sup> D. van der Marel, J. van Elp, G. A. Sawatzky, and D. Heitmann, Phys. Rev. B37, 5136 (1988).

<sup>38</sup> L. H. Tjeng, C. T. Chen, and S-W. Cheong, Phys. Rev. B 45, 8205 (1992).

<sup>39</sup> R. Bar-Deroma, J. Felsteiner, R. Brener, J. Ashkenazi and D. van der Marel Phys. Rev. B 45, 2361 (1992).

<sup>40</sup> Daniel I. Khomskii, Section 12.10, Basic Aspects of the Quantum Theory of Solids, Cambridge University Press (2010), ISBN-13 978-0-511-78832-1 (eBook).

<sup>41</sup> E. Koch, The Physics of Correlated Insulators, Metals, and Superconductors Modeling and Simulation Vol. 7, E. Pavarini, E. Koch, R. Scalettar, and R. Martin (eds.), Forschungszentrum Julich, (Julich 2017). ISBN 978-3-95806-224-5.

<sup>42</sup> M. Schluter, M. S. Hybertsen, and N. E. Christensen, Physica C 153-155, 1217 (1988); M. S. Hybertsen, M. Schluter, and N. E. Christensen, Phys. Rev. B 39, 9028 (1989).

<sup>43</sup> H. Eskes, G. A. Sawatzky, and L. F. Feiner, Physica C 160, 424(1989).

<sup>44</sup> A. K. McMahan, J. F. Annett and R. M. Martin, Cuprate parameters from numerical Wannier functions, Phys. Rev. B 42, 6268 (1990).

<sup>45</sup> P. Werner, R. Sakuma, F. Nilsson, and F. Aryasetiawan, Phys. Rev. B 91, 125142 (2015).

<sup>46</sup> M. Hirayama, Y. Yamaji, T. Misawa and M. Imada, Phys. Rev. B 98, 134501 (2018).

<sup>47</sup> Kung, Y. F. et al. Characterizing the three-orbital Hubbard model with determinant quantum Monte Carlo. Phys. Rev. B 93, 155166 (2016).

<sup>48</sup> R. Coldea, S. M. Hayden, G. Aeppli, T. G. Perring, C. D. Frost, T. E. Mason, S.-W. Cheong, and Z. Fisk, Phys. Rev. Lett. 86, 5377(2001).

<sup>49</sup> P. W. Leung, B. O. Wells, and R. J. Gooding, Phys. Rev. B 56, 6320 (1997).

<sup>50</sup> C. Kim, P. J. White, Z.-X. Shen, T. Tohyama, Y. Shibata, S. Maekawa, B. O. Wells, Y. J. Kim, R. J. Birgeneau, and M. A. Kastner, Phys. Rev. Lett. 80, 4245 (1998).

<sup>51</sup> R. Neudert, S.-L. Drechsler, J. Malek, H. Rosner, M. Kielwein, Z. Hu, M. Knupfer, M. S. Golden, J. Fink, N. Nucker, M. Merz, S. Schuppler, N. Motoyama, H. Eisaki, S. Uchida,

M. Domke and G. Kaindl, Four-band extended Hubbard Hamiltonian for the one-dimensional cuprate  $\text{Sr}_2\text{CuO}_3$  : Distribution of oxygen holes and its relation to strong intersite Coulomb interaction, *Phys. Rev. B* 62, 10652 (2000).

<sup>52</sup> K. Okada and A. Kotani, *J. Phys. Soc. Jpn.* 66, 341 (1997).

<sup>53</sup> High-resolution x-ray-photoemission study of single crystalline  $\text{Sr}_2\text{CuO}_2\text{Cl}_2$  T. Boske, O. Knauff, R. Neudert, M. Kielwein, M. Knupfer, M. S. Golden, and J. Fink, H. Eisaki and S. Uchida K. Okada, A. Kotani, *Phys. Rev. B* 56, 3438 (1997).

<sup>54</sup> M. A. van Veenendaal, H. Eskes, and G. A. Sawatzky, *Phys. Rev. B* 47, 11462 (1993).

<sup>55</sup> M. A. van Veenendaal and G. A. Sawatzky, Nonlocal Screening Effects in 2p X-Ray Photoemission Spectroscopy Core-Level Line Shapes of Transition Metal Compounds, *Phys. Rev. Lett.* 70, 2459 (1993).

<sup>56</sup> K. Okada and A. Kotani, *J. Phys. Soc. Jpn.*, 74, 653 (2005).

<sup>57</sup> N. Nucker, E. Pellegrin, P. Schweiss, J. Fink, S. L. Molodtsov, C. T. Simmons, G. Kaindl, W. Frentrup, A. Erb and G. Muller-Vogt, *Phys. Rev. B* 51, 8529(1995).

<sup>58</sup> Andrzej M. Oles and Wojciech Grzelka, Electronic structure and correlations of  $\text{CuO}_3$  chains in  $\text{YBa}_2\text{Cu}_3\text{O}_7$ , *Phys. Rev. B* 44, 9531(1991).

<sup>59</sup> M. A. van Veenendaal, G. A. Sawatzky, and W. A. Groen, Electronic structure of  $\text{Bi}_2\text{Sr}_2\text{Ca}_{1-x}\text{Y}_x\text{CuO}_{8+\delta}$ . Cu 2p x-ray-photoelectron spectra and occupied and unoccupied low-energy states, *Phys. Rev B* 49, 1407 (1994).

<sup>60</sup> A. C. Walters, T. G. Perring, J.-S. Caux, A. T. Savici, G. D. Gu, C.-C. Lee, W. Ku and I. A. Zaliznyak, Effect of covalent bonding on magnetism and the missing neutron intensity in copper oxide compounds, *Nat. Phys.* 5, 867 (2009).

<sup>61</sup> P. Bourges, H. Casalta, A. S. Ivanov, and D. Petitgrand, *PRL* 79, 4906 (1997).

<sup>62</sup> S.M. Hayden, G. Aeppli, T.G. Perring, H.A. Mook, and F. Dogan, *Phys. Rev. B* 54, R6905 (1996).

<sup>63</sup> M. P. M. Dean et al. High-energy magnetic excitations in the cuprate superconductor  $\text{Bi}_2\text{Sr}_2\text{CaCuO}_{8+\delta}$  : Towards a unified description of its electronic and magnetic degrees of freedom. *Phys. Rev. Lett.* 110, 147001 (2013).

<sup>64</sup> Peng, Y. Y. et al. Magnetic excitations and phonons simultaneously studied by resonant inelastic x-ray scattering in optimally doped  $\text{Bi}_{1.5}\text{Pb}_{0.55}\text{Sr}_{1.6}\text{La}_{0.4}\text{CuO}_{6+\delta}$ , *Phys. Rev. B* 92, 064517 (2015).

<sup>65</sup> Lichen Wang, Guanhong He, Zichen Yang, Mirian Garcia-Fernandez, Kejin Zhou, Matteo Minola, Matthieu Le Tacon, Bernhard Keimer, Abhishek Nag, Yingying Peng and Yuan Li, Paramagnons and high-temperature superconductivity in a model family of cuprates, *Nat. Comm.* 13:3163(2022) <https://doi.org/10.1038/s41467-022-30918-z>.

<sup>66</sup> Y. Y. Peng, E. W. Huang, R. Fumagalli, M. Minola, Y. Wang, X. Sun, Y. Ding, K. Kummer, X. J. Zhou, N. B. Brookes, B. Moritz, L. Braicovich, T. P. Devereaux, and G. Ghiringhelli, Dispersion, damping, and intensity of spin excitations in the monolayer  $(\text{Bi},\text{Pb})_2(\text{Sr},\text{La})_2\text{CuO}_{6+\delta}$  cuprate superconductor family, *Phys. Rev. B* 98, 144507 (2018).

<sup>67</sup> S. Johnston, F. Vernay and T. P. Devereaux, Impact of an oxygen dopant in  $\text{Bi}_2\text{Sr}_2\text{CaCu}_2\text{O}_{8+\delta}$ , *Europhys. Lett.* 86, 37007 (2009).

<sup>68</sup> H. Jacobsen, S. M. Gaw, A. J. Princep, E. Hamilton, S. Toth, R. A. Ewings, M. Enderle, E. M. Hetrov Wheeler, D. Prabhakaran, and A. T. Boothroyd, Spin dynamics and exchange interactions in  $\text{CuO}$  measured by neutron scattering, *Phys. Rev. B* 97, 144401 (2018).

<sup>69</sup> E. Zurek, O. Jepsen, and O. K. Andersen, *ChemPhysChem* 6, 1934 (2005).

<sup>70</sup> Lipscombe, O. J., Hayden, S. M., Vignolle, B., McMorrow, D. F. and Perring, T. G. Persistence of high-frequency spin fluctuations in overdoped superconducting  $\text{La}_{2-x}\text{Sr}_x\text{CuO}_4$  ( $x = 0.22$ ). *Phys. Rev. Lett.* 99, 067002 (2007).

<sup>71</sup> L. Braicovich, et al. Magnetic excitations and phase separation in the underdoped  $\text{La}_{2-x}\text{Sr}_x\text{CuO}_4$  superconductor measured by resonant inelastic x-ray scattering. *Phys. Rev. Lett.* 104, 077002 (2010).

<sup>72</sup> M. P. M. Dean et al. Spin excitations in a single  $\text{La}_2\text{CuO}_4$  layer. *Nature Mater.* 11, 850?854 (2012).

<sup>73</sup> G. Levy, M. Yaari, T. Z. Regier, and A. Keren, Experimental determination of superexchange energy from two-hole spectra, *Cond-mat arXiv:2107.09181v1* (2021).